Thermodynamic modelling of the Fe-Sn-Zr system based on new experiments and first- principles calculations

Paul Lafaye, Caroline Toffolon-Masclet, Jean-Claude Crivello, Jean-Marc Joubert

Thermodynamic modelling of the Fe–Sn–Zr system based on new experiments and first-principles calculations

Paul Lafaye[a,b,*], Caroline Toffolon-Masclet [a], Jean-Claude Crivello[b], Jean-Marc Joubert[b**]

[a]DEN-Service de Recherches Métallurgiques Appliquées, CEA, Université Paris-Saclay, F-91191 Gif-sur-Yvette, France

[b] ICMPE, UPEC-CNRS, 94320, Thiais, France

[**] corresponding author

Tel.: +33 1 49 78 13 44; Fax: +33 1 49 78 12 03

E-mail address: joubert@icmpe.cnrs.fr

Abstract

The Fe–Sn–Zr system has been studied by first principles calculation and modelled with the Calphad method using the literature and new experimental data. The work includes a revision of Fe–Sn and Fe–Zr systems. Our experimental study has confirmed that the W_5Si_3 phase (stoichiometry $Zr_5Sn_{2,3}Fe_{0,7}$) is stable at 1350 °C but also down to 1000 °C. Moreover, the crystal structure of the *X*'' phase has been determined. The formation enthalpies of all the ordered configurations of the *C*15, *C*16, *C*36, *E*1a phases and the stoichiometric Fe_5Sn_3, Fe_3Sn_2, FeSn, $FeSn_2$, $Fe_{23}Zr_6$, $FeSn_2Zr_6$ (θ), $Fe_{36.36}Sn_{36.36}Zr_{27.27}$ (*N*) et $Fe_{14.39}Sn_{43.47}Zr_{39.13}$ (*X*'') compounds have been calculated using the Density Functional Theory (DFT). The mixing enthalpies of the *A*1, *A*2 and *A*3 binary solid solutions have been calculated using the Special Quasirandom Structures (SQS) and DFT calculation. From these new experimental and calculated data, new thermodynaùic assessments are proposed for Fe–Sn, Fe–Zr and Fe–Sn–Zr systems.

*Present affiliation : Centre de Recherche en Calcul Thermochimique (CRCT), Polytechnique Montréal, Montréal, Québec, H3C 3A7, Canada

Keywords: Fe–Sn–Zr; Calphad; DFT; SQS; thermodynamic assessment; phase equilibrium

1. Introduction

The Fe–Sn–Zr system is a system of great interest particularly for the nuclear industry both for low and high temperature applications. Regarding the low temperature applications, Zr–rich alloys (Zircaloy-4) containing Fe and Sn as major alloying elements have been employed for fuel cladding and as structural components in Light Water Reactors (LWR) and Heavy Water Reactors (HWR). Similarly for high temperature applications, Fe–Zr alloys are involved in the Fe–Zr–U–O quaternary system for in-vessel Corium studies [1].

At last, Fe–Zr alloys are promising candidate for hydrogen storage, particularly Fe_2Zr intermetallic compound because of its good gravimetric storage capacity, and the fast kinetics of hydrogen absorption–desorption and low equilibrium pressure at room temperature as well [2].

Several Calphad description of the Fe–Zr system are available in the literature [3–7]. Most of them [3–6] were obtained without DFT calculations and the resulting assessed formation enthalpies exhibit large deviations from the DFT ones. Moreover, recent papers devoted to DFT calculations of the Fe–Zr binary system [8,9] exhibit erroneous conclusions concerning the stability of the *C*16 and the $Fe_{23}Zr_6$ phases. Thus, several recent publications [7,10,11] consider the $Fe_{23}Zr_6$ phase as stable despite the existence of several studies demonstrating its unstability [9,12–14].

Similarly, the Calphad modelling of the Fe–Sn and Sn–Zr systems available in the literature have been carried out without DFT calculations [15,16] and the corresponding ground-states strongly disagree with our calculated energy level.

Thus, new thermodynamic assessments of the Fe–Sn, Fe–Zr and Sn–Zr systems are necessary. The Calphad description of the Sn–Zr system has been published separately in a paper dedicated to the Cr–Nb–Sn–Zr quaternary system [17]. We present here new Calphad assessments of the Fe–Sn and Fe–Zr binary systems and the description of the Fe–Sn–Zr ternary system. We provide new experimental results on the Fe–Sn–Zr ternary system concerning the stability of the W_5Si_3 phase (stoichiometry $Zr_5Sn_{2,3}Fe_{0,7}$) based on a comparison with the recent results of Calta *et al.* [18] in the Fe–Sn–Hf system. The formation enthalpies of the *C*15, *C*16, *C*36, *E*1a phases and the stoichiometric Fe_5Sn_3, Fe_3Sn_2, FeSn, $FeSn_2$, $Fe_{23}Zr_6$, $FeSn_2Zr_6$ (θ), $Fe_{36.36}Sn_{36.36}Zr_{27.27}$ (*N*) et $Fe_{14.39}Sn_{43.47}Zr_{39.13}$ (*X*'') compounds have been calculated using the Density Functional Theory (DFT). The SQS method is used with DFT calculations in order to calculate the enthalpies of mixing of the *A*1, *A*2 and *A*3 binary solid solutions. The first part of this paper is dedicated to the literature survey of the different systems; the second part is dedicated to the methodology and the third part to our results.

2. Literature survey

2.1 The Fe–Sn binary system

2.1.1 Experimental data

The Fe–Sn system presents four intermetallic phases, Fe_5Sn_3, Fe_3Sn_2, FeSn and $FeSn_2$. The phase diagram also includes two eutectoid reactions as well as one monotectic reaction. One may note the presence of a miscibility gap in the liquid phase below 1370 °C [19].

The invariant reactions were measured by Mills *et al.* [20], Tréheux *et al.* [21] and Fedorenko *et al.* [22]. The liquidus has been measured by Isaac *et al.* [23], Arita *et al.* [24], Predel *et al.* [19] in the Fe-rich part and by Isaac *et al.* [23], Arita *et al.* [24], Predel *et al.* [19] and Campbell *et al.* [25] in the Sn-rich. The miscibility gap in the liquid phase was measured

by Shiraishi *et al.* [26], Mills *et al.* [20], Campbell *et al.* [25], Predel *et al.* [19] and Nunoue *et al.* [27]. The solubility of the Fe-rich bcc solid solution was mainly studied by Mills *et al.* [20], Yamamoto *et al.* [28] and Arita *et al.* [24].

2.1.2 Thermodynamic data

The formation enthalpies of the FeSn and $FeSn_2$ compounds have been measured by electromotive force by Eremenko *et al.* [29] and Zabdyr *et al.* [30]. Measurements of Fe and Sn activities in the liquid phase have been performed by Yazawa *et al.* [31], Shiraishi *et al.* [26], Wagner *et al.* [32], Fedorenko *et al.* [22], Yamamoto *et al.* [33] and more recently by Nunoue *et al.* [27]. The mixing enthalpy of the liquid phase was measured by Wagner *et al.* [32], Petrushevski *et al.* [34], Yamamoto *et al.* [33] and Lueck *et al.* [35]. Note that the mixing enthalpies of the solid solutions have never been determined.

2.1.3 Thermodynamic assessment

The Fe–Sn system has been assessed by many authors [15,36–38]. The most recent study was carried out by Huang *et al.*[38] considering all experimental data available in the literature except for the mixing enthalpies of the liquid phase measured by Petrushevski *et al.* [34].

2.2 The Fe–Zr binary system

2.2.1 Experimental data

The Fe–Zr system has been experimentally investigated by many authors [39–49]. The Zr-rich part of the diagram was first studied by Hayes *et al.* [39] and corrected by Tanner *et al.* [40] using X-ray diffraction (XRD). The *C*16 phase was first reported by Malakhova *et al.* [41] as a stable phase down to 0 K, Malhakhova *et al.* [42] and Aubertin *et al.* [43] have confirmed this result. The Fe-rich part of the phase diagram was investigated by Svechnikov *et al.*[44].

Borrelly *et al.*[45] determined the solubility in the different solid solutions. The phase diagram was reviewed in the whole composition range by Alekseeva *et al.* [46]. Later, Bhanumurthy *et al.* [47,48] and Kumar *et al.* [49] reported the *C*16 phase to be a high temperature stable phase. Servant *et al.* [3] reinvestigated the invariant reaction temperatures as well as the melting temperature of the *C*15 phase. A detailed review and a very careful reinvestigation of the whole composition range of this system has been carried out by Stein *et al.* [14] using metallography, XRD, EPMA and DTA measurements. These authors have shown that the presumed $Fe_{23}Zr_6$ compound stable at high temperature is actually an oxygen stabilized compound. Indeed, in binary alloys, this compound always appears as third phase which is not complying with the Gibbs phase rule. Moreover, the precipitate size and the amount of the $Fe_{23}Zr_6$ phase remains unchanged by increasing the heat treatment duration. At last, these authors have clearly shown that $Fe_{23}Zr_6$ precipitates specifically in regions with high O content. Moreover, Stein *et al.* [14] have demonstrated that the hexagonal *C*36 polymorph of the Laves phase is a high-temperature stable phase. According to Stein *et al.* [14] this system exhibits eight condensed phases (Liquid, *A*1, *A*2, *A*3, *C*15, *C*16, *C*36 and *E*1a). Two intermetallic compounds are stable at low temperatures (*C*15 and *E*1a). This system is characterised by the presence of one congruent melting and three eutectic, three eutectoid, two peritectic and one peritectoid invariant reactions.

2.2.2 Thermodynamic data

Sudavtsova *et al.* [50], Sidorov *et al.*[51], Wang *et al.*[52] and Rösner-Kuhn *et al.* [53] have measured the mixing enthalpies in the liquid phase at different temperatures. Moreover, Rösner-Kuhn *et al.* [53] also measured the formation enthalpy of the *C*15 phase as well as Gachon *et al.*[54]. The heat capacity of *C*15 phase was provided by Lück *et al.*[55]. Servant *et al.* [3] measured the enthalpy of melting of the *C*15 phase.

Later, the DFT calculations performed by Barberis *et al.*[12] and Ohodnicki *et al.*[13] showed that the formation enthalpies of the *C*16 and $Fe_{23}Zr_6$ phases are not on the convex hull and these authors concluded that these phases are not stable down to 0 K. More recently, Lumley *et al.* [56] calculated the Fe–Zr ground-state not including the $Fe_{23}Zr_6$ phase. Their results confirmed that the *C*16 phase is not stable down to 0 K. Tao *et al* [8] have calculated the formation enthalpy of the *C*16 phase. These authors concluded on the stability of this phase only considering the negative value of the formation enthalpy. This conclusion is not appropriate as long as the complete the ground-state has not been calculated. In addition, a new first-principles study dealing with DFT calculations on the Fe–Zr system was provided by Ali *et al.* [9]. The authors have calculated the formation enthalpies and the electronic structure of the *C*15, *C*16, *C*36 and *E*1a phases. Unfortunately, their conclusions on the stability of the $Fe_{23}Zr_6$ compound are improper. Indeed, a negative value of formation enthalpy is a necessary but not sufficient condition to conclude whether the compound is stable or not. Contrariwise, their calculations clearly exhibit that the formation enthalpy of the $Fe_{23}Zr_6$ compound is by 0.8 kJ/mol more positive than the calculated convex hull.

2.2.3 Thermodynamic assessment

Pelton [57] was the first author to model the Fe–Zr system mainly based on experimental determination of the phase diagram and measurement of the formation enthalpy of the *C*15 phase [54]. Servant *et al.* [3] reinvestigated the Calphad modelling of the Fe–Zr system according to their new measurements of the temperatures of invariant reactions as well as the fusion enthalpy of the *C*15 phase. Later, Jiang *et al.* [4], Guo *et al.* [6] and Rigaud *et al.* [5] performed new thermodynamic description of the system mainly based on new experimental measurement of Stein *et al.* [14]. Taking into account new DFT calculations available on the

Fe–Zr system [12,13], Yang *et al.* [7] carried out a new Calphad modelling of the system but did not find clear evidence to confirm about the phase stability of $Fe_{23}Zr_6$.

2.3 The Fe–Sn–Zr ternary system

2.3.1 Experimental data

The first studies of this system were carried out by Tanner *et al.* [58] and Korotkova [59] in the Zr-rich part of the phase diagram. These two authors have reported the existence of the θ phase, which structure has been solved by Kwon *et al.* [60], as being K_2UF_6. In addition, Kwon *et al.* [60] have reported the existence of the $Zr_5Sn_{2.3}Fe_{0.7}$ phase at 1350 ° C. The reported structure is an ordered variant of W_5Si_3 obtained by splitting of the site 4*a* of the space group *I*4/*mcm* into sites 2*a* and 2*b* of space group *I*422. Mazet *et al.* [61] have reported the existence of the Fe_6Sn_6Zr compound which crystallizes in the $MgFe_6Ge_6$ structure (also called $HfFe_6Ge_6$). More recently, Nieva *et al.* [62] studied this system in a wider composition range. In addition to the *θ* phase, these authors reported two other ternary phases, called *X* and *N*, without succeeding in solving their structures. An experimental study in the Zr-poor *X* part of the Fe–Sn–Zr system was performed by Savidan *et al.* [63] who reported a complete isothermal section at 900 °C. These authors have confirmed the existence of the Fe_6Sn_6Zr ternary phase but also highlighted two new ternary phases, the *Y* and *C*36 phases. Moreover, they established that two different phases were involved within the homogeneity domain of the *X* phase, called *X*' and *X*". In addition, Savidan *et al.* [63] solved the *N* phase structure. At last, Nieva *et al.* [64] determined the isothermal section at 800 °C of this system.

Very recently, Calta *et al.* [18] solved the structure of the $Hf_9Fe_4Sn_{10}$ compound and have noted several similarities between the structures of the Fe–Sn–Zr and Fe–Sn–Hf ternary compounds.

2.3.2 Thermodynamic data

No paper reports measured or calculated thermodynamic data for this system.

2.3.3 Thermodynamic assessment

There is no thermodynamic assessment available in the literature.

3. Methodology

3.1 Experimental details

The experimental procedure was identical to that employed in our previous work [17]. The samples have been synthesized from pieces of the pure elements (Fe from Neyco (99.99%), Sn from Alfa Aesar (99.8%) and Zr "Van Arkel" (55 ppm of oxygen) from LTMEX-CEA)) by arc melting under argon atmosphere. The alloys were melted five times and turned upside down between each melting to ensure homogeneity. The weight losses were less than 1 wt.%. The samples were wrapped in molybdenum foils and sealed in a silica tube under argon and then annealed in a resistance furnace. A part of the samples was examined by X-ray powder diffraction (XRD) at room temperature using a Bruker D8 diffractometer equipped with a graphite monochromator in the diffracted beam with Cu Kα radiation. The diffractogram was treated with a Rietveld analysis. Another part of the samples was polished and served for the Electron Microprobe Analysis (EPMA, Cameca SX100) using pure elements as standards

3.2 DFT calculations

The enthalpies of formation of the *C*15 ($Fd\bar{3}m$), *C*16 (*I*4/*mcm*), *C*36 ($P6_3/mmc$), *E*1a (*Cmcm*) phases and the stoichiometric Fe_5Sn_3 ($P6_3/mmc$), Fe_3Sn_2 ($R\bar{3}m$), FeSn (*P*6/*mmm*), $FeSn_2$ (*I*4/*mcm*), $Fe_{23}Zr_6$ ($Fm\bar{3}m$), $FeSn_2Zr_6$ (θ), $Fe_{36.36}Sn_{36.36}Zr_{27.27}$ (*N*) et $Fe_{14.39}Sn_{43.47}Zr_{39.13}$ (*X*'') compounds have been calculated using VASP code [65,66]. The procedure was similar to that used in our previous work [17] including the calculation of all

the configurations obtained by distributing the atoms in the *C*15 and *C*36 structures. The same code ZenGen [67], potentials [68] k-points meshing (16 x 16 x 16 for $Fe_{23}Zr_6$, 21 x 6 x 8 for *E*1a) and Blöchl corrections [69] was used. With respect to the magnetic state of Fe, the calculations are performed with spin polarization. The reference for enthalpies is the Stable Element Reference (SER, ground-state structure for Fe-bcc, β–Sn for Sn and Zr-hcp).

SQS calculations [70] were also conducted in the same way as previously [17] with *A*1, *A*2 and *A*3 structures taken from the literature [71] and complemented by 1/16 and 15/16 dilutions

3.3 Calphad methodology

The Gibbs energy of each phase is written:

$$G_m^\alpha = {}^{ref}G_m^\alpha + {}^{id}G_m^\alpha + {}^{ex}G_m^\alpha$$

where ${}^{ref}G_m^\alpha$ is the Gibbs energy surface of reference. Considering a phase α modelled with two-SL in a $A-B-C$ ternary system, ${}^{ref}G_m^\alpha$ can be formulated as:

$${}^{ref}G_m^\alpha = y_A^{(1)}y_A^{(2)}G_{A:A} + y_A^{(1)}y_B^{(2)}G_{A:B} + y_A^{(1)}y_C^{(2)}G_{A:C} + y_B^{(1)}y_A^{(2)}G_{B:A} + y_B^{(1)}y_B^{(2)}G_{B:B}$$
$$+ y_B^{(1)}y_C^{(2)}G_{B:C} + y_C^{(1)}y_A^{(2)}G_{C:A} + y_C^{(1)}y_B^{(2)}G_{C:B} + y_C^{(1)}y_C^{(2)}G_{C:C}$$

With $G_{i:j} = H_{i:j}^{SER,\alpha} - T * S_{i:j}$; $y_j^{(s)}$ is the site occupancy of each constituent on each sublattice and $H_{i,j}^{SER,\alpha}$ is the 0 K formation enthalpy and $S_{i:j}$ is the formation entropy of the ordered configuration.

${}^{id}G_m^\alpha$ is the molar Gibbs energy of an ideal mixing, based on the number of possible arrangements of the constituents of the phase:

$${}^{id}G_m^\alpha = RT\sum_{s=1}^{s=2} a_s \sum_i y_i^{(s)} \ln(y_i^{(s)})$$

R is the gas constant and $a_s$the multiplicity of the sublattice s.

The last term of the Gibbs energy is the excess Gibbs energy that includes all the non-ideal mixing contributions:

$$^{E}G_m^{\alpha} = y_A^{(1)}y_B^{(1)}y_C^{(2)}L_{A,B:C}^{\alpha} + y_A^{(1)}y_B^{(2)}y_C^{(2)}L_{A:B,C}^{\alpha} + y_A^{(1)}y_B^{(2)}y_C^{(1)}L_{A,C:B}^{\alpha} + y_A^{(2)}y_B^{(1)}y_C^{(1)}L_{B,C:A}^{\alpha} + y_A^{(2)}y_B^{(1)}y_C^{(2)}L_{B:A,C}^{\alpha} + y_A^{(2)}y_B^{(2)}y_C^{(1)}L_{C:A,B}^{\alpha}$$

where the excess parameters $L_{i,j:k}^{\alpha}$ can be expressed as a Redlich-Kister polynomial.

Table 1 presents the different phases treated within the Compound Energy Formalism and the corresponding sublattice model chosen according to the crystal structures.

At last, just note that the DFT calculations we performed are used as input data in the Calphad modelling. Thus, similarly to any experimental data, we provide systematic comparison between our DFT calculations and our optimization (labelled "calc." and "opt.", respectively, in Figures 1, 2, 5, 6 and Tables 2 and 3).

4. Results and discussion

4.1 The Fe–Sn system

4.1.1 First-principles calculations

Fig. 1 shows the 0 K calculated formation enthalpies of the *end-members* of the *C*15 and *C*36 Laves phases and the stoichiometric Fe_5Sn_3, Fe_3Sn_2, FeSn and $FeSn_2$ compounds compared with data from literature. The calculated formation enthalpies of the stoichiometric Fe_5Sn_3, Fe_3Sn_2, FeSn and $FeSn_2$ compounds are also reported in the Table 2. The calculated mixing enthalpies of the *A*1 and *A*2 solid solutions are reported in Fig. 2 and Table 3 and compared with our and former assessments.

4.1.2 Thermodynamic modelling

4.1.2.1 Selection of data

The liquidus measurements performed by Isaac *et al.* [23], Predel *et al.* [19] and Campbell *et al.* [25] were considered. The measurements of Arita *et al.* [24] were rejected because of the large deviations with the other sets of data.

The different measurements of the miscibility gap in the liquid phase exhibit relatively large discrepancies as reported in Figure 3. Hari Kumar *et al.* [15] have modelled a critical point of the miscibility gap at 1612 K but have noted that it could be at a higher temperature, which was confirmed by Okamoto [72] and Huang *et al.* [38]. Moreover, Okamoto [72] suggested that the miscibility gap is symmetrical. Thus, we have considered the measurements performed by Predel *et al.* [19] which exhibit a symmetrical miscibility gap in the liquid phase and a temperature of the critical point superior to the one modelled by Hari Kumar *et al.* [15]. Note that the miscibility gap modelled by Miettinen *et al.* [37] and Huang *et al.* [38] is in good agreement with the measurements of Predel *et al.* [19].

The Sn solubility in the bcc solid solution were taken from Mills *et al.* [20] and Arita *et al.* [24]. The solubility determined by Yamamoto *et al.* [33] were rejected due to the important disagreements with the other data.

The invariant reaction temperatures and compositions determined by Tréheux *et al.* [21] were considered.

The Gibbs free energy of the FeSn and $FeSn_2$ compounds measured by Eremenko *et al.* [29] and Zabdyr *et al.* [30] were rejected because of the strong disagreement with our own DFT calculations as reported in Figure 1. Our DFT calculations of the formation enthalpies of the intermetallic phases and the mixing enthalpies of the fcc and bcc solid solutions were considered.

At last, note that the Fe and Sn activity measured by Yamamoto *et al.* [33] and Nunoue *et al.* [27] were considered. The mixing enthalpy of the liquid phase measured by Yamamoto *et al.* [33] and Lueck *et al.* [35] was also considered.

4.1.2.2 Calphad assessment

We optimized the interaction parameters of the liquid phase according to the liquidus, the miscibility gap and the mixing enthalpy of the liquid phase. Binary second order parameters have been optimized without temperature dependence.

The formation enthalpies of the intermetallic compounds have been optimized after the measurements performed by Tréheux *et al.* [21] and our own calculations. The formation enthalpies of the end-members of the *C*15 and *C*36 Laves phases not existing in this system were kept fixed to DFT values. No entropic term was used for the Laves phases.

The bcc solid solution was modelled using regular and sub-regular binary interaction parameters with temperature dependence for the regular parameter. The fcc solid solution has been described with a regular interaction parameter without temperature dependence.

4.1.2.3 Discussion

Our thermodynamic assessment of the Fe–Sn system was performed using less parameters than Huang *et al.* [38]. Our description shows a comparable agreement with the experimental data similarly to Huang *et al.* [38] as reported in Figure 3. One may note that the ground state we have optimized is in very good agreement with our DFT calculations contrary to the description of Huang *et al.* [38] who considered the measurements performed by Eremenko *et al.* [29] and Zabdyr *et al.* [30], as reported in Figure 1. The optimized mixing enthalpy of the bcc solid solution shows a slightly better agreement with our calculations than the one assessed by Huang *et al.* [38], as reported in Figure 2.

At last, one may note the good agreement between the Fe and Sn activities measured by Yamamoto *et al*. [33] and Nunoue *et al*.[27]. The calculation we performed is reported in Figure 4 and optimized parameters are given in Table 4.

4.2 The Fe–Zr system

4.2.1 First-principles calculations

Fig. 5 shows the 0 K calculated formation enthalpies of the *end-members* of *C*15, *C*16, *C*36, *E*1a and $Fe_{23}Zr_6$ phases, compared to data from literature. The calculated formation enthalpies of the *end-members* of *C*15 and *C*36 at the stoichiometry Fe_2Zr are reported in Table 2. The calculated mixing enthalpies of the in the solid solutions are reported in Fig. 6 and Table 3 and compared with our and former assessments.

The calculated ground-state of the Fe–Zr system allows us confirming the results of Barberis *et al.*[12] and Ohodnicki *et al.*[13] that the *C*16 and $Fe_{23}Zr_6$ compounds are not stable down to 0 K since the calculated formation enthalpies of these two phases are above the calculated ground states line (mixing of *C*14 + *E*1a at the 1:2 and 23:6 compositions respectively).

4.2.2 Thermodynamic modelling

4.2.2.1 Selection of data

Compositions and temperature of the invariant reactions, the measurements of the single-phase and two-phase equilibria in addition to the liquidus were taken from the work of Stein *et al.* [14]. The data obtained by these authors are considered as the most accurate measurements available for this phase diagram. Thus, due to the very careful work of Stein *et al.* [14] confirmed by Barberis *et al.*[12], Ohodnicki *et al.*[13], Lumley *et al.*[56] and the DFT calculations we performed, the $Fe_{23}Zr_6$ phase was not included in the thermodynamic modelling of the system. Moreover, the *C*36 phase was considered instead of the $Fe_{23}Zr_6$ compound as a high-temperature phase, according to the work of Stein *et al.* [14]. We have considered the formation enthalpy of the stable *C*15 phase measured by Rösner-Kuhn *et al.* [53] and Gachon *et al.*[54] and the ground-state calculated by Barberis *et al.*[12],

Ohodnicki *et al.*[13], Lumley *et al.*[56], Ali *et al.* [9] and that obtained in the present work. The mixing enthalpies of the liquid phase measured by Sudavtsova *et al.* [50], Sidorov *et al.*[51], Wang *et al.*[52] and Rösner-Kuhn *et al.* [53] were considered as well as the mixing enthalpies of the *A*1, *A*2 and *A*3 solid solutions obtained in this paper.

4.2.2.2 Calphad assessment

The formation enthalpy of the stable *C*15, *C*16, *C*36 and *E*1a *end-members* has been optimized after literature data [9,12,13,53,54] and our calculations. On the other hand, the formation enthalpy of the metastable *end-members* was kept fixed to the DFT values. Furthermore, no entropic term was used for the metastable *end-members*. The values of mixing enthalpies of the *A*1, *A*2 and *A*3 solid solutions were optimised after both the literature data [14,45] and our calculations.

The solubilities of the *A*1 and *A*3 terminal solid solutions were described using regular binary interaction parameters without temperature dependence. The solubilities of the *A*2 terminal solid solution were described using regular and sub-regular binary interaction parameters with temperature dependence for the regular parameter. The homogeneity range of the *C*15 Laves phase was described using a regular binary interaction parameter without temperature dependence. The liquid phase was described using regular and subregular interaction parameters without temperature dependence optimised considering the measurements available in the literature [50–53].

The optimized mixing enthalpy of the liquid phase is reported in Fig. 7 and compared with the measurements of Sudavtsova *et al.* [50], Sidorov *et al.*[51], Wang *et al.*[52] and Rösner-Kuhn *et al.* [53].

Fig. 8 shows the good description of the experimental data points obtained by our calculated diagram using our set of parameters. The optimized parameters are given in Table 5.

4.2.2.3 Discussion

Our thermodynamic description of the Fe–Zr system has been done using less parameters than the one of Guo *et al.* [6].

The optimized ground-state of the Fe–Zr system shown in Fig. 5 is in good agreement with the measurements [53,54] and calculations [9,12,13] available in the literature and with our own DFT calculations. Moreover, the optimised mixing enthalpies of the *A*1, *A*2 and *A*3 solid solutions exhibit a good agreement with our SQS calculations as reported in Fig. 6. At last, one may note the reasonable agreement existing between the optimised mixing enthalpy of the liquid phase and the measurements available in the literature [50–53] as reported in Fig. 7.

Our description of the Fe–Zr phase diagram exhibits a better agreement with the experimental data points than the one of Guo *et al.* [6] particularly for the liquid phase in the whole composition range and for the bcc solid solution on the Zr-rich part.

4.3 The Fe–Sn–Zr system

4.3.1 Experimental study

Table 6 summarizes the chemical composition, annealing treatment and the structure and composition of the different phases of the Fe–Sn–Zr samples synthesized in the present work. Concerning the W_5Si_3 (*I*4/*mcm*) phase, the almost constant phase composition observed as function of both the nominal composition and the temperature indicates the absence of any homogeneity range.

From the Rietveld analysis, the distribution of Sn and Fe of the W_5Si_3 (*I*4/*mcm*) phase at 1350 ° C is found to be similar to that proposed by Kwon *et al.* [60]. At 1000 °C, the distribution is more homogeneous between sites 2*a* and 2*b* and the structure is therefore very similar to that of W_5Si_3. Note that, at 1000 °C, this phase is involved in three phase equilibria with Zr_5Sn_3 phase (Mn_5Si_3 crystal structure) and a third phase close to the $ZrFe_2$ composition.

However, the structure of this third phase could not be solved. The structure of this phase is not a Laves phase, nor any other structure identified in the ternary Fe–Sn–Zr system. In addition, note that the proportion of this phase increases with the Fe content.

In a recent paper, Calta *et al.* [18] determined the structure of $Hf_9Fe_{4-x}Sn_{10+x}$. We discovered that the structure of the *X*" phase that remained unknown after the work of Savidan *et al.* [63] was isotypic with this phase. Figure 9 presents the Rietveld refinement of the sample $Fe_{19.2}Sn_{43.2}Zr_{37.6}$ (corresponding to the sample 8 in the work of Savidan *et al.* [63]). The composition is indeed very close to that of the Hf phase. The presence of the additional $ZrSn_2$ (13%) and *N* (22%) phases already shown in previous work was confirmed from the Rietveld refinement. Given the complexity of the crystal structure, no attempt was made to refine atomic coordinates and/or site occupancies.

In the course of the refinement (and subsequent DFT calculation), we found an error in the Table 3 of Ref. [18]. After checking this point with the authors, we assumed that the z coordinate for Sn(5) is 0.0000 instead of 0.2695.

4.3.2 First-principles calculations

Table 7 summarizes the ternary intermetallic phases of the Fe–Sn–Zr system, their crystallographic description as well as the value of the calculated and optimized formation enthalpy for the $FeSn_2Zr_6$ (θ), $Fe_{36.36}Sn_{36.36}Zr_{27.27}$ (*N*) and $Fe_{14.39}Sn_{43.47}Zr_{39.13}$ (*X*") compounds. The formation enthalpy of the $Fe_{17.65}Sn_{39.22}Zr_{43.13}$ (*X*') and $Fe_{36.36}Sn_{36.36}Zr_{27.2}$ (*Y*) compounds is not calculated in this paper because their crystal structure is not known. In Fig. 10, we have reported the calculation of the formation enthalpies of the end-members of the Mn_5Si_3 and W_5Si_3 structures.

4.3.3 Thermodynamic modelling

At first, note that the phase equilibria determined by Nieva *et al.* [62,64] and Savidan *et al.* [63] were considered. The formation enthalpies of the ternary intermetallic phases were fixed at the values computed by DFT, the entropic terms of the $FeSn_2Zr_6$ (θ), $Zr_5Sn_{2.3}Fe_{0.7}$ and $Fe_{36.36}Sn_{36.36}Zr_{27.2}$ (Y) phases were optimized. The homogeneity range of the Laves phases were optimized using two ternary interaction parameters for the $C36$ phase and one for the $C15$ phase.

The result of our modelling is the best compromise between all measured phase equilibria. We have reported the calculated isothermal section together with experimental data of the ternary system at 800 °C, 900 °C, 1000 °C and 1350 °C in figures 11 to 14. The optimized parameters are given in Table 8.

4.3.3.4 Discussion

The competition between the Mn_5Si_3 and W_5Si_3 structures reported in figure 10 shows that the W_5Si_3 structure is more stable than the Mn_5Si_3 structure only slightly and only in a small range of composition in quite good agreement with the measurements of Kwon *et al.* [60] and those obtained in the frame of this work. This, together with the absence of an homogeneity range, justifies that the phase is treated as a stoichiometric one.

Our thermodynamic modelling of the Fe–Sn–Zr system is in good agreement with the measurements performed by Nieva *et al.* [62,64], Savidan *et al.* [63] and our own measurements as shown in Figure 11 to 14. Some of the slight differences observed between the isothermal sections at 800 °C and 900 °C [62] like the shift in the tie-triangle [Fe(α) – Y – $C36$] toward Sn-richer composition as well as the shift in the tie-triangle [Fe(α) – $C15$ – $C36$] toward Sn-poorer composition were reproduced in our modelling. The calculated isothermal sections at 1000 °C and 1350 °C show that the W_5Si_3 structure is stable in good agreement with experimental measurements. Moreover, at 900 °C, the calculated isothermal section is in

good agreement with the experimental isothermal section provided by Nieva *et al.* [62,64]. The solubility of Fe in the η-phase of the Sn–Zr system and the ternary extension of the θ phase were not taken into account in the modelling.

In the absence of other isothermal sections, liquidus projection and temperatures for the ternary invariant reactions, the description should be considered as only tentative.

5. Conclusions

The experimental study we have performed on the Fe–Sn–Zr ternary system has confirmed that the W_5Si_3 phase (stoichiometry $Zr_5Sn_{2.3}Fe_{0.7}$) is stable at 1350 °C but also down to 1000 °C. Moreover, the crystal structure of the *X*" phase has been determined using XRD and Rietveld refinement.

The Fe–Sn–Zr system has been then studied by first-principles calculations. We carried out new DFT calculations of the formation enthalpies of the *C*15, *C*16, *C*36, *E*1a phases and the stoichiometric Fe_5Sn_3, Fe_3Sn_2, FeSn, $FeSn_2$, $Fe_{23}Zr_6$, $FeSn_2Zr_6$ (θ), $Fe_{36.36}Sn_{36.36}Zr_{27.27}$ (*N*) et $Fe_{14.39}Sn_{43.47}Zr_{39.13}$ (*X*'). Our results clearly show that the $Fe_{23}Zr_6$ phase is not thermodynamically stable down to 0 K. Moreover, the competition between the two different structures W_5Si_3 and Mn_5Si_3 has been investigated. We have shown that the W_5Si_3 is only stable in a narrow range of composition close to the stoichiometry $Zr_5Sn_2Fe_1$.

At last, the thermodynamic modelling of the Fe–Sn and Fe–Zr binary system as well as the Fe–Sn–Zr ternary systems has been performed using the Calphad approach according to our new experimental results and DFT calculations. One may note that the ground-state of the modelled Fe–Sn binary system has been strongly shifted from the former assessments available in the literature [15].

Acknowledgements

Eric Bouaravong and Didier Hamon contributed to the alloy synthesis and the EPMA measurements. The authors aknowledge HPC resources from GENCI-CINES (Grant 2018-096175 and den0006) used for the DFT calculations, the GDR CNRS n°3584 TherMatHT for fruitful discussions and collaborative work on the present project andthe French Tripartite Institute CEA/EDF/Framatome [Projet Gaine] for funding.

References

[1] C. Guéneau, V. Dauvois, P. Pérodeaud, C. Gonella, O. Dugne, Liquid immiscibility in a (O,U,Zr) model corium, J. Nucl. Mater. 254 (1998) 158–174.
[2] L. Rodrigo, J.A. Sawicki, Aging characteristics of Zr-V-Fe getters as observed by Mossbauer spectroscopy, J. Nucl. Mater. 265 (1999) 208–212.
[3] C. Servant, C. Gueneau, I. Ansara, Experimental and thermodynamic assessment of the FeZr system, J. Alloys Compd. 220 (1995) 19–26.
[4] M. Jiang, K. Oikawa, T. Ikeshoji, L. Wulff, K. Ishida, Thermodynamic calculations of Fe-Zr and Fe-Zr-C systems, J. Phase Equilibria. 22 (2001) 406–417.
[5] V. Rigaud, B. Sundman, D. Daloz, G. Lesoult, Thermodynamic assessment of the Fe–Al–Zr phase diagram, Calphad. 33 (2009) 442–449.
[6] C. Guo, Z. Du, C. Li, B. Zhang, M. Tao, Thermodynamic description of the Al–Fe–Zr system, Calphad. 32 (2008) 637–649.
[7] Y. Yang, L. Tan, H. Bei, J.T. Busby, Thermodynamic modeling and experimental study of the Fe–Cr–Zr system, J. Nucl. Mater. 441 (2013) 190–202.
[8] X. Tao, J. Zhu, H. Guo, Y. Ouyang, Y. Du, Phase stability, thermodynamic and mechanical properties of $AlZr_2$, $FeZr_2$ and Al_2FeZr_6 from first-principles calculations, J. Nucl. Mater. 440 (2013) 6–10.
[9] K. Ali, A. Arya, P.S. Ghosh, G.K. Dey, A first principles study of cohesive, elastic and electronic properties of binary Fe-Zr intermetallics, Comput. Mater. Sci. 112 (2016) 52–66.
[10] W.L. Huang, Y. Yu, S.Y. Yang, C.P. Wang, X.J. Liu, R. Kainuma, K. Ishida, Experimental Investigation of Phase Equilibria in the Cu-Fe-Zr Ternary System, J. Phase Equilibria Diffus. 34 (2013) 438–446.
[11] S.Y. Yang, J.B. Zhang, C.P. Wang, W.J. Yu, Z. Shi, X.J. Liu, Experimental investigation of phase equilibria in the Ni-Fe-Zr ternary system, J. Mater. Res. 31 (2016) 2407–2414.
[12] P. Barberis, N. Dupin, C. Lemaignan, A. Pasturel, J.M. Grange, Microstructure and phase control in Zr-Fe-Cr-Ni alloys: Thermodynamic and kinetic aspects, in: P. Rudling, B. Kammenzind (Eds.), Zircon. Nucl. Ind. 14th Int. Symp., American Society Testing and Materials, W Conshohocken, 2005: pp. 129–156.
[13] P.R. Ohodnicki, N.C. Cates, D.E. Laughlin, M.E. McHenry, M. Widom, Ab initio theoretical study of magnetization and phase stability of the $(Fe,Co,Ni)_{23}B_6$ and $(Fe,Co,Ni)_{23}Zr_6$ structures of $Cr_{23}C_6$ and $Mn_{23}Th_6$ prototypes, Phys. Rev. B. 78 (2008) 144414-13.

[14] F. Stein, G. Sauthoff, M. Palm, Experimental determination of intermetallic phases, phase equilibria, and invariant reaction temperatures in the Fe-Zr system, J. Phase Equilibria. 23 (2002) 480–494.
[15] K.C.H. Kumar, P. Wollants, L. Delaey, Thermodynamic evaluation of Fe-Sn phase diagram, Calphad. 20 (1996) 139–149.
[16] R.J. Perez, C. Toffolon-Masclet, J.-M. Joubert, B. Sundman, The Zr-Sn binary system: New experimental results and thermodynamic assessment, Calphad-Comput. Coupling Phase Diagr. Thermochem. 32 (2008) 593–601.
[17] P. Lafaye, C. Toffolon-Masclet, J.-C. Crivello, J.-M. Joubert, Experimental investigations and thermodynamic modelling of the Cr–Nb–Sn–Zr system, Calphad-Comput. Coupling Phase Diagr. Thermochem. 64 (2019) 43-54.
[18] N.P. Calta, M.G. Kanatzidis, $Hf_3Fe_4Sn_4$ and $Hf_9Fe_{(4-x)}Sn_{(10+x)}$: Two stannide intermetallics with low-dimensional iron sublattices, J. Solid State Chem. 236 (2016) 130–137.
[19] B. Predel, M. Frebel, Precipitation behavior of α-solid solutions of the Fe-Sn system, Metall. Trans. 4 (1973) 243–249.
[20] K.C. Mills, E.T. Turkdogan, Liquid miscibility gap in iron–tin system, Trans Met. Sot AIME. 230 (1964) 1202-1203.
[21] D. Treheux, D. Duc, P. Guiraldenq, Determination of the Limits of Solubility of Tin in Alpha and Gamma Irons, Mem Sci Rev Met. 71 (1974) 289–293.
[22] A.N. Fedorenko, V.G. Brovkin, Vapor pressure of tin and thermodynamic properties of the tin–iron system, Sb Nauchn Tr Gos Proektn Nauchno-Issled Inst Gipronikel. 3 (1977) 83-89.
[23] E. Isaac, G. Tammann, On the alloys of iron with tin and gold, Z Anorg Chem. 53 (1907) 281–297.
[24] M. Arita, M. Ohyama, K.S. Goto, M. Someno, Measurements of activity, solubility and diffusivity in alpha and gamma Fe-Sn alloys between 1183 and 1680 K, Z. Fuer Met. Res. Adv. Tech. 72 (1981) 244–250.
[25] A.N. Campbell, J.H. Wood, G.B. Skinner, The System Iron-Tin: Liquidus Only, J. Am. Chem. Soc. 71 (1949) 1729–1733.
[26] S.V. Shiraishi, H.B. Bell, Thermodynamic study of tin smelting. 1. Iron–tin and iron–tin–oxygen alloys, Inst Min. Met Trans Sect C. 77 (1968) 104–105.
[27] S. Nunoue, E. Kato, Mass Spectrometric Determination of the Miscibility Gap in the Liquid Fe-Sn System and the Activities of This System at 1 550°C and 1 600°C, Tetsu-Hagane. 73 (1987) 868–875.
[28] T. Yamamoto, T. Takashima, K. Ishida, Inter-diffusion in the alpha-solid solution of the Fe–Sn system, J. Jpn. Inst. Met. 45 (1981) 985-990.
[29] V.N. Eremenko, Conditions for the formation of stannides by the interaction of iron with Sn-Pb melts, and their thermodynamic properties, Izv. Akad. Nauk SSSR Met. 4 (1976) 58–62.
[30] L. Zabdyr, K. Fitzner, Gibbs free energy of formation of iron antimonide (FeSb2), iron–tin (FeSn), and iron–tin ($FeSn_2$) intermetallic phases, Arch Hutn. 29 (1984) 227–233.
[31] A. Yazawa, K. Koike, Tin smelting. II. Activity measurements in molten tin–iron alloy, Nippon Kogyo Kaishi. 85, 969, (1969) 39-42.
[32] S. Wagner, G.R. St.Pierre, Thermodynamics of the liquid binary iron-tin by mass spectrometry, Metall. Trans. 3 (1972) 2873–2878.
[33] M. Yamamoto, S. Mori, E. Kato, Mass spectrometric study of the thermodynamic properties of liquid Fe-Sn, Fe-Sn-Cu alloys, Tetsu-Hagane Journal Iron Steel Inst. Jpn. 67 (1981) 1952–1961.

[34] M.S. Petrushevskii, Y.O. Esin, V.M. Baev, P.V. Gel'd, Influence of short-range ordering on the concentration-dependence of the enthalpies of formation of liquid iron-tin alloys, Rus. Met. 1 (1978) 61-63.
[35] R. Lueck, B. Predel, Enthalpy of mixing of liquid Iron-Tin alloys determined by means of a new high-temperature calorimeter, Z. Fuer Met. Res. Adv. Tech. 76 (1985) 684–686.
[36] H.D. Nüssler, O. von Goldbeck, P.J. Spencer, A thermodynamic assessment of the iron-tin system, Calphad. 3 (1979) 19–26.
[37] J. Miettinen, Thermodynamic description of the Cu–Fe–Sn system at the Cu–Fe side, Calphad. 32 (2008) 500–505.
[38] Y.-C. Huang, W. Gierlotka, S.-W. Chen, Sn–Bi–Fe thermodynamic modeling and Sn–Bi/Fe interfacial reactions, Intermetallics. 18 (2010) 984–991.
[39] E. Hayes, A. Roberson, W. Obrien, Constitution and Mechanical Properties of Zirconium-Iron Alloys, Trans. Am. Soc. Met. 43 (1951) 888–905.
[40] L. Tanner, D. Levinson, Observations on the System Zirconium Iron, Trans. Am. Inst. Min. Metall. Eng. 215 (1959) 1066–1067.
[41] T. Malakhova, Z. Alekseyeva, The Zr-Fe Phase-Diagram in the Range 20 - 40 at-Percent Fe and the Crystalline-Structure of the Intermetallic Compound Zr_3Fe, J. -Common Met. 81 (1981) 293–300.
[42] T. Malakhova, A. Kobylkin, The Zr-Fe Phase-Diagram (0-66.6 at.% Fe), Russ. Metall. (1982) 187–191.
[43] F. Aubertin, U. Gonser, S. Campbell, H. Wagner, An Appraisal of the Phases of the Zirconium-Iron System, Z. Met. 76 (1985) 237–244.
[44] V.N. Svechnikov, A.T. Spektor, The Iron-Zirconium Phase Diagram, Proc Acad Sci USSR Chem Sect. 142 (1962) 231–233.
[45] R. Borrelly, P. Merle, Study by Electron-Diffraction of Precipitation in Low Iron Content Zr-Fe Alloys, J. Nucl. Mater. 173 (1990) 105–107.
[46] Z. Alekseeva, N. Korotkova, The Zr-Fe Phase-Diagram, Russ. Metall. (1989) 197–203.
[47] K. Bhanumurthy, G. Kale, S. Khera, Reaction Diffusion in the Zirconium Iron System, J. Nucl. Mater. 185 (1991) 208–213.
[48] K. Bhanumurthy, G. Kale, Modification of Zirconium-Iron Phase-Diagram, Scr. Metall. Mater. 28 (1993) 753–756.
[49] L. Kumar, R.V. Ramanujan, R. Tewari, P. Mukhopadhyay, S. Banerjee, Active eutectoid decomposition in Zr-3 wt.% Fe, Scr. Mater. 40 (1999) 723–728.
[50] V.S. Sudavtsova, V.P. Kurach, G.I. Batalin, Thermochemical properties of liquid binary alloys Fe-(Y, Zr, Nb, Mo), Izv. Akad. Nauk SSSR Met. (1987) 60–61.
[51] O.Y. Sidorov, M.G. Valishev, Y.O. Esin, P.V. Gel'd, Formation heat of iron-zirconium melts, Izv Akad Nauk SSSR Met. 6 (1988) 23–25.
[52] H. Wang, R. Luck, B. Predel, Calorimetric Determination of the Enthalpy of Mixing of Liquid Iron-Zirconium Alloys, Z. Met. 81 (1990) 843–846.
[53] M. Rösner-Kuhn, J. Qin, K. Schaefers, U. Thiedemann, M.G. Frohberg, Temperature dependence of the mixing enthalpy and excess heat capacity in the liquid system iron-zirconium, Z. Für Met. 86 (1995) 682–685.
[54] J. Gachon, J. Hertz, Enthalpies of Formation of Binary Phases in the Systems Feti, Fezr, Coti, Cozr, Niti, and Nizr, by Direct Reaction Calorimetry, Calphad-Comput. Coupling Phase Diagr. Thermochem. 7 (1983) 1–12.
[55] R. Luck, H. Wang, Heat-Capacity of the Fe2zr Intermetallic Compound, J. Alloys Compd. 191 (1993) 11–12.

[56] S.C. Lumley, S.T. Murphy, P.A. Burr, R.W. Grimes, P.R. Chard-Tuckey, M.R. Wenman, The stability of alloying additions in Zirconium, J. Nucl. Mater. 437 (2013) 122–129.
[57] A. Pelton, L. Leibowitz, R. Blomquist, Thermodynamic Analysis of Phase-Equilibria in the Iron Zirconium System, J. Nucl. Mater. 201 (1993) 218–224.
[58] L. Tanner, D.W. Levinson, The system zirconium–iron–tin, Trans ASM. 52 (1960) 1115–1136.
[59] N.V. Korotkova, The zirconium corner of the phase diagram Zr–Sn–Fe, Russ Met. 5 (1990) 201–208.
[60] Y. Kwon, S. Sevov, J.D. Corbett, Substituted W_5Si_3- and Zr_6Al_2Co-type phases formed in the zirconium-antimony and zirconium–tin systems with iron group metals, Chem. Mater. 2 (1990) 550–556.
[61] T. Mazet, B. Malaman, Local chemical and magnetic disorder within the $HfFe_6Ge_6$-type RFe_6Sn_6 compounds (R = Sc, Tm, Lu and Zr), J. Magn. Magn. Mater. 219 (2000) 33–40.
[62] N. Nieva, D. Arias, Experimental partial phase diagram of the Zr–Sn–Fe system, J. Nucl. Mater. 359 (2006) 29–40.
[63] J.-C. Savidan, J.-M. Joubert, C. Toffolon-Masclet, An experimental study of the Fe–Sn–Zr ternary system at 900 °C, Intermetallics. 18 (2010) 2224–2228.
[64] N. Nieva, C. Corvalán, M.J. Jiménez, A. Gómez, C. Arreguez, J.-M. Joubert, D. Arias, Phase diagram of the Fe-Sn-Zr system at 800 °C, J. Nucl. Mater. 487 (2017) 186–191.
[65] G. Kresse, J. Furthmüller, Efficient iterative schemes for ab initio total-energy calculations using a plane-wave basis set, Phys. Rev. B. 54 (1996) 11169–11186.
[66] G. Kresse, D. Joubert, From ultrasoft pseudopotentials to the projector augmented-wave method, Phys. Rev. B. 59 (1999) 1758–1775.
[67] J.-C. Crivello, R. Souques, A. Breidi, N. Bourgeois, J.-M. Joubert, ZenGen, a tool to generate ordered configurations for systematic first-principles calculations: The Cr–Mo–Ni–Re system as a case study, Calphad. 51 (2015) 233–240.
[68] J.P. Perdew, K. Burke, M. Ernzerhof, Generalized Gradient Approximation Made Simple, Phys. Rev. Lett. 77 (1996) 3865–3868.
[69] P. Blöchl, Projector augmented-wave method, Phys. Rev. B. 50 (1994) 17953-17979.
[70] A. Zunger, S.-H. Wei, L.G. Ferreira, J.E. Bernard, Special quasirandom structures, Phys. Rev. Lett. 65 (1990) 353–356.
[71] C. Jiang, C. Wolverton, J. Sofo, L.-Q. Chen, Z.-K. Liu, First-principles study of binary bcc alloys using special quasirandom structures, Phys. Rev. B. 69 (2004) 214202-10.
[72] H. Okamoto, Binary alloy phase diagrams, in: 2nd ed. Ohio: ASM International, 1990: p. 1774.
[73] S.V. Shiraishi, H.B. Bell, Thermodynamic study of tin smelting. 1. Iron–tin and iron–tin–oxygen alloys, Inst Min. Met Trans Sect C. 77 (1968) 104–105.
[74] X. Tao, J. Zhu, H. Guo, Y. Ouyang, Y. Du, Phase stability, thermodynamic and mechanical properties of $AlZr_2$, $FeZr_2$ and Al_2FeZr_6 from first-principles calculations, J. Nucl. Mater. 440 (2013) 6–10.
[75] E.P. Abrahamson, S.L. Lopata, Trans.Metall.Soc.AIME. 236 (1966) 76–87.

Figure caption:

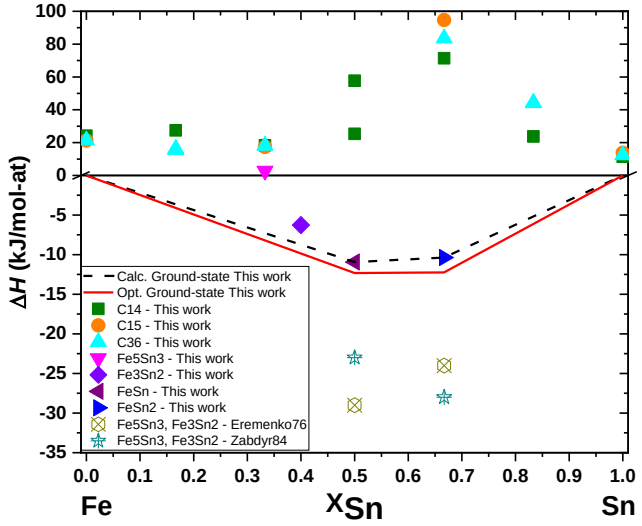

Figure 1: Calculated formation enthalpies of the intermetallic phases of the Fe–Sn system compared to data of Eremenko *et al.* [29] and Zabdyr *et al.* [30]

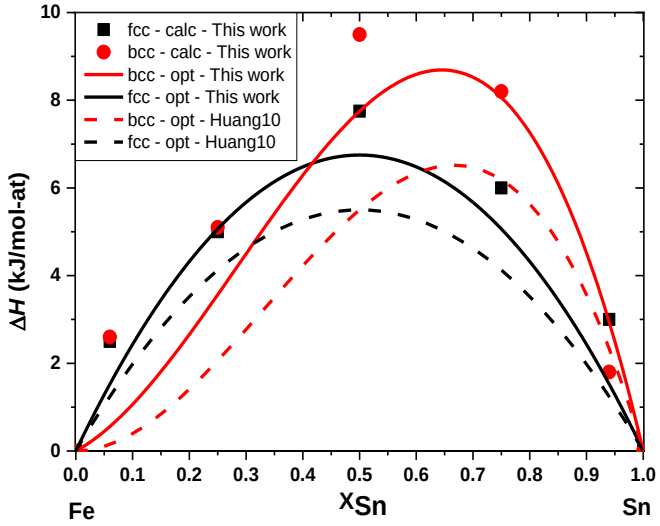

Figure 2: Calculated mixing enthalpies of the *A*1 and *A*2 solid solutions in the Fe–Sn system compared to data of Huang *et al.* [38].

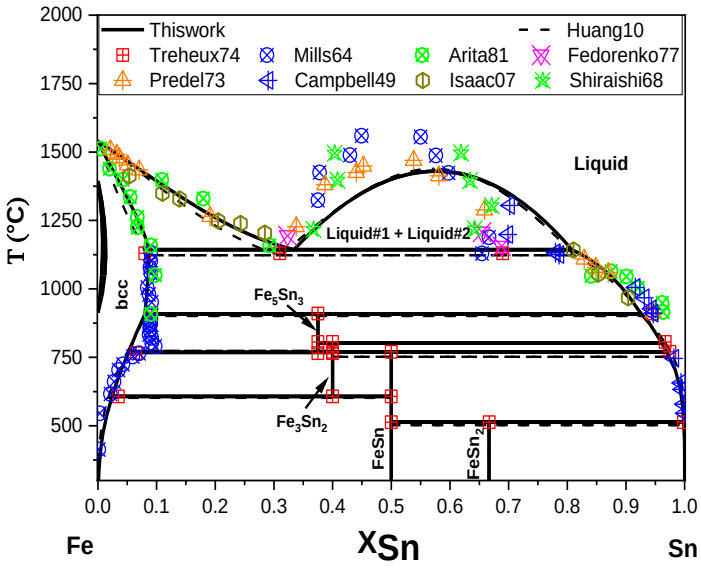

Figure 3: Calculated Fe-Sn system compared to data of Tréheux *et al.* [21], Arita *et al.* [24], Mills *et al.* [20], Shiraishi *et al.* [73], Predel *et al.* [19], Campbell *et al.* [25], Isaac *et al.* [23] et Fedorenko *et al.* [22] and assessment of Huang *et al.* [38].

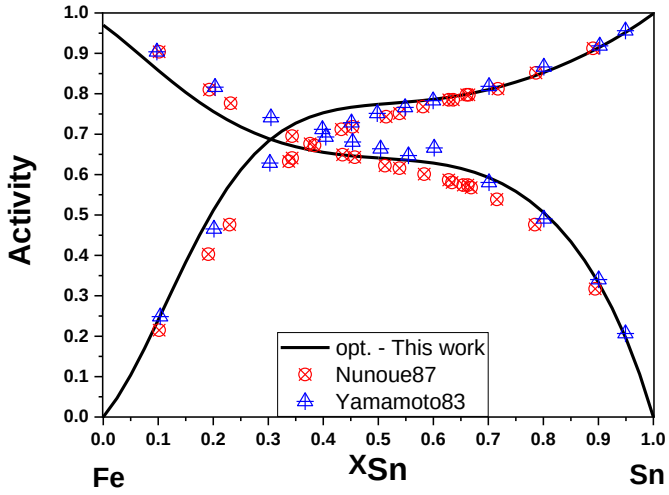

Figure 4: Calculated activities of Fe and Sn at 1600 °C compared to data of Nunoue *et al.* [27] and Yamamoto *et al.* [33]

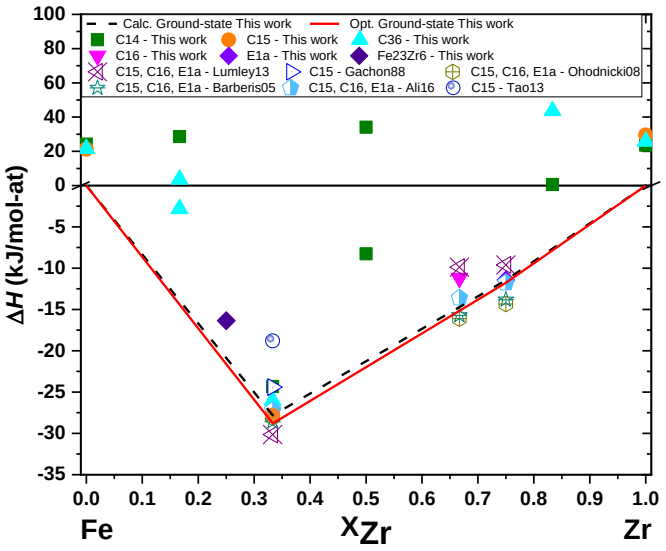

Figure 5: Calculated formation enthalpies of the intermetallic phases of the Fe–Zr system compared to data of Gachon *et al.* [54], Barberis *et al.* [12], Ohodnicki *et al.* [13], Tao *et al.* [74], Lumley *et al.* [56] et Ali *et al.* [9].

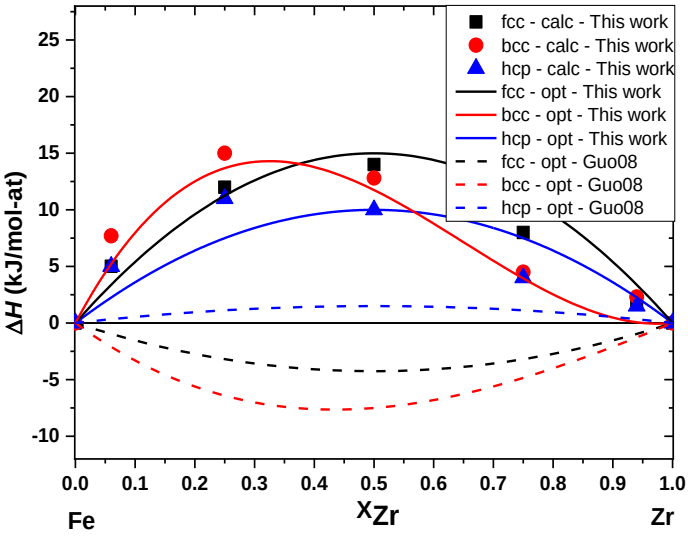

Figure 6: Calculated mixing enthalpies of the *A*1, *A*2 and *A*3 solid solutions in the Fe–Zr system compared to data of Guo *et al.* [7].

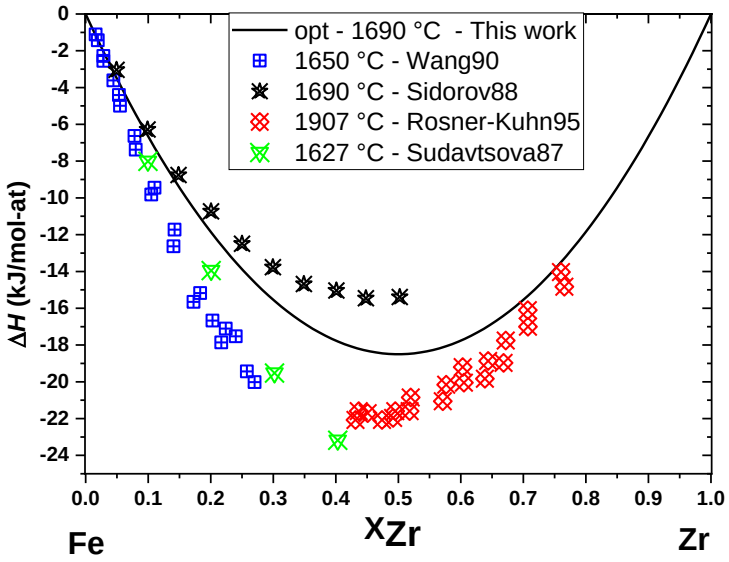

Figure 7: Calculated mixing enthalpies of the liquid phase at 1690 °C in the Fe–Zr system compared to data of Sudatsova *et al.* [50], Sidorov *et al.*[51], Wang *et al.*[52] and Rösner-Kuhn *et al.* [53].

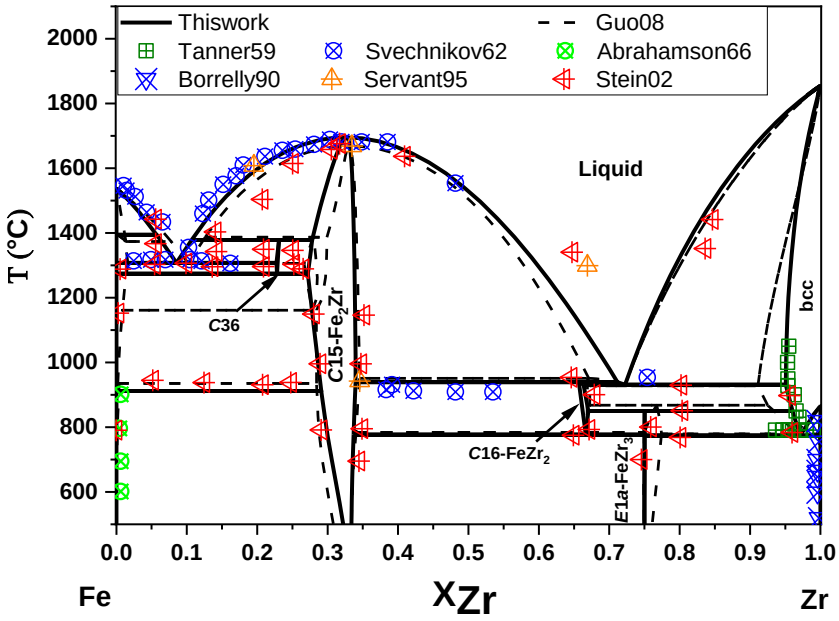

Figure 8: Calculated Fe–Zr system compared to data of Tanner *et al.* [40], Svechnikov *et al.* [44], Abrahamson *et al.* [75], Borrelly *et al.* [45], Servant *et al.* [3] et Stein *et al.* [14] and assessment of Guo *et al.* [6].

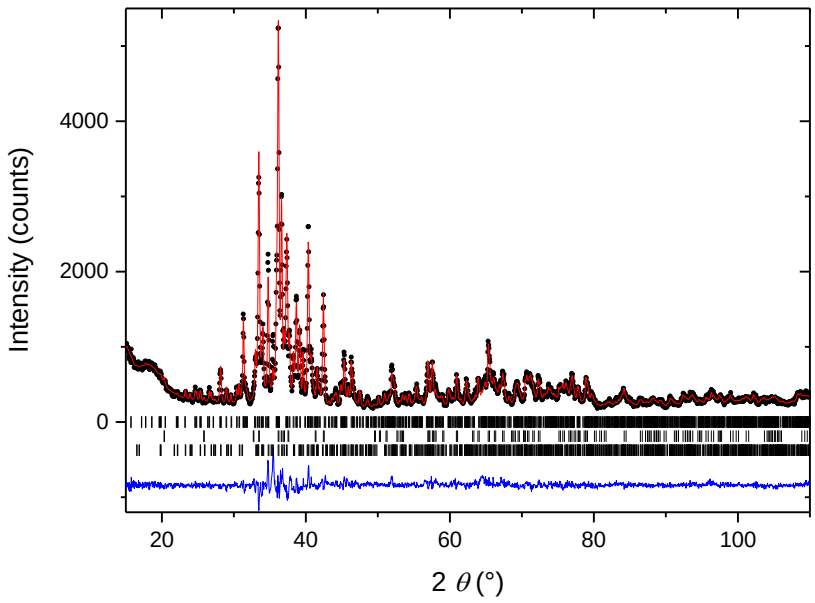

Figure 9: Rietveld refinement of $Fe_{19.2}Sn_{43.2}Zr_{37.6}$ (sample 8 in Ref. [63], χ^2=2.9, R_B(X")=6%). Experimental (points), calculated (line) and difference (line below) patterns are shown. The markers show the positions of the different reflections of *X*" ($Hf_9Fe_{4-x}Sn_{10+x}$ type) (top), $ZrSn_2$ ($TiSi_2$ type) (middle) and N ($Sc_3Mn_2Ga_6$ type) (bottom).

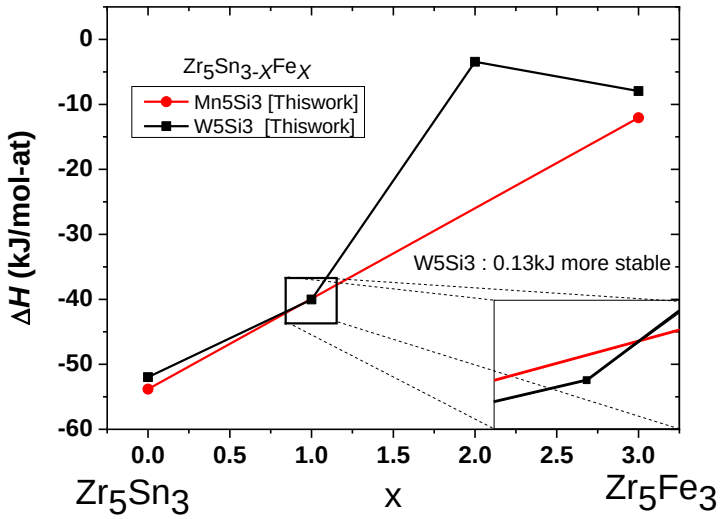

Figure 10: DFT calculated formation enthalpies of the Mn_5Si_3 and W_5Si_3 end-members

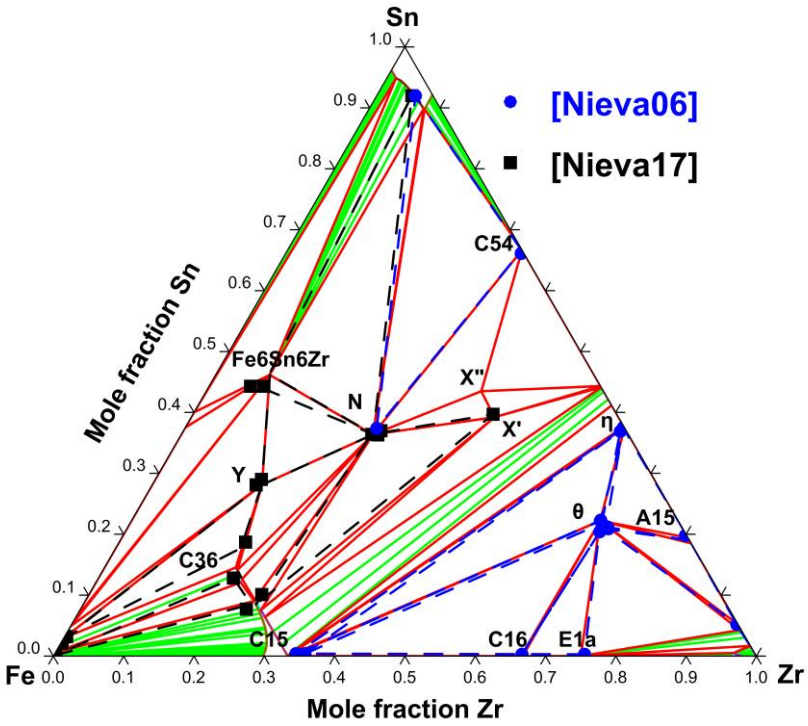

Figure 11: Calculated isothermal section at 800 °C of the Fe–Sn–Zr system compared to experimental data of Nieva *et al.* [62, 64].

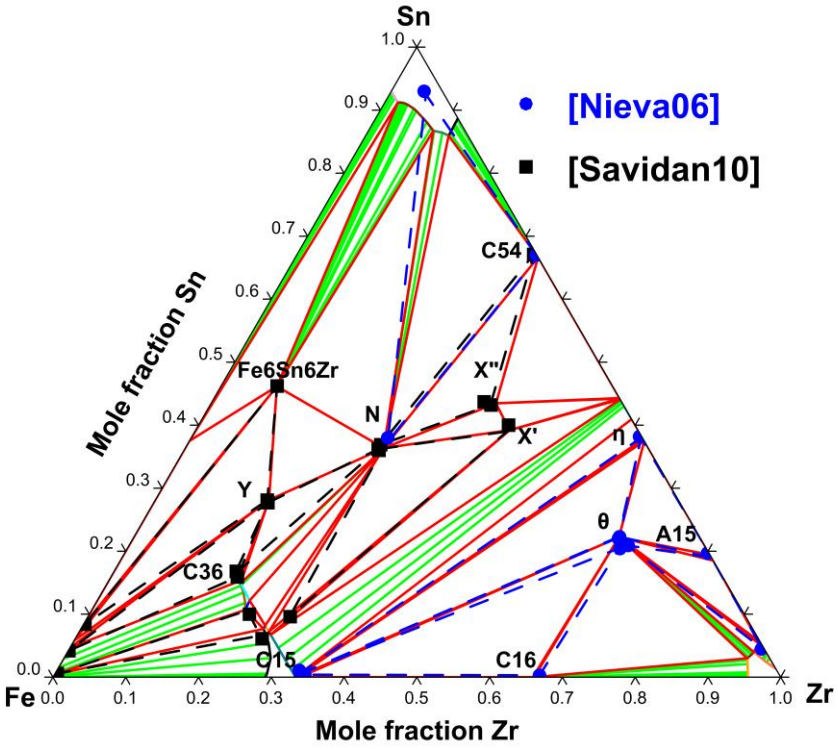

Figure 12: Calculated isothermal section at 900 °C of the Fe–Sn–Zr system compared to experimental data of Savidan *et al.* [63] and Nieva *et al.* [62].

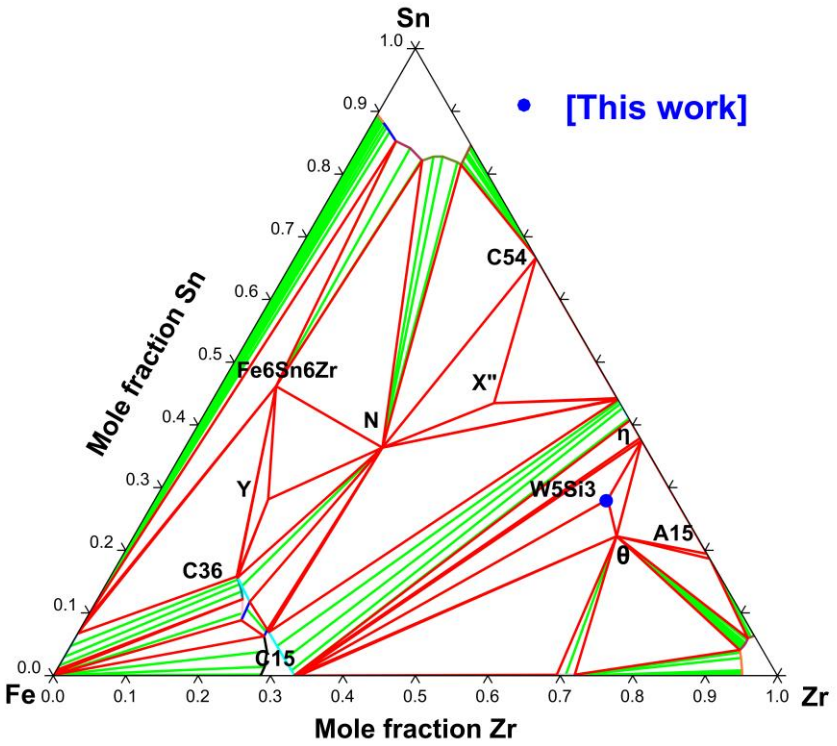

Figure 13: Calculated isothermal section at 1000 °C of the Fe–Sn–Zr system

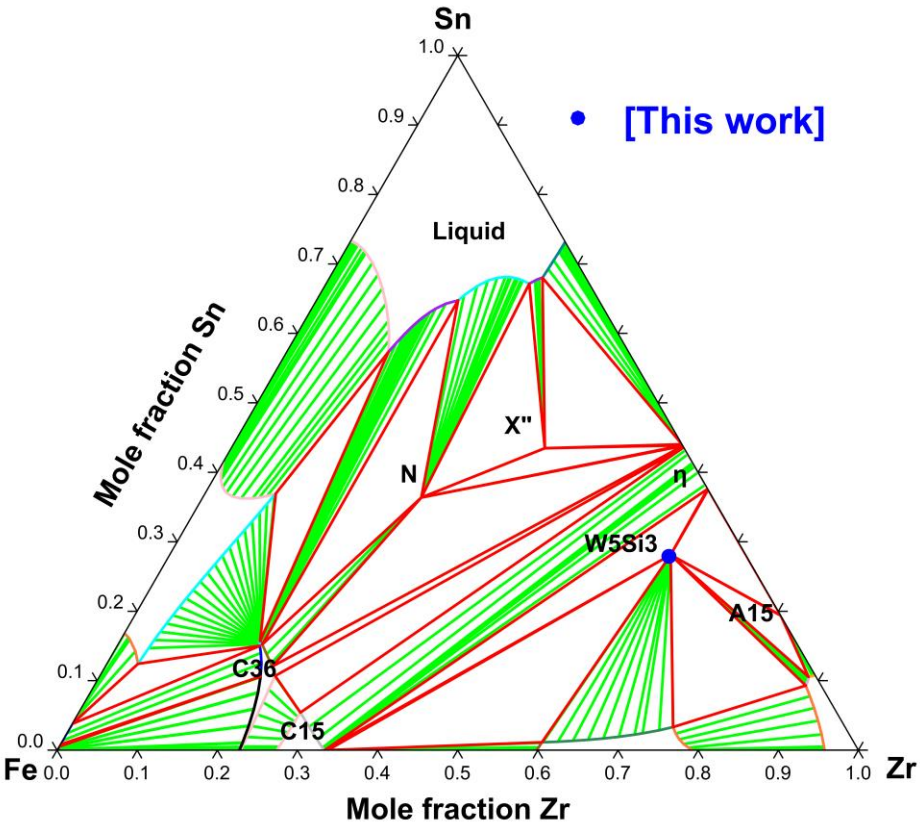

Figure 14: Calculated isothermal section at 1350 °C of the Fe–Sn–Zr system

Table caption:

Table 1: Crystallographic description and sublattice model of the non-stoichiometric phases of the Fe–Sn–Zr and Fe–Zr system

Phase	Space group	Wyckoff position	Crystallographic site	Sublattice modelling
*C*15	*Fd*-3*m* (227)	8*a*; 16*d*	2	$(Fe,Sn,Zr)_2\,(Fe,Sn,Zr)_1$
*C*16	*I*4/*mcm* (140)	4a; 8*h*	2	$(Fe,Zr)_1\,(Fe,Zr)_2$
*C*36	$P6_3/mmc$ (194)	4*e*; 4*f;* 4*f;* 8*i; !*8*i*	3	$(Fe,Sn,Zr)_4\,(Fe,Sn,Zr)_4\,(Fe,Sn,Zr)_{16}$
*E*1a	*Cmcm* (63)	4*c;* 4*c* ; 8*f*	3	$(Fe,Zr)\,(Fe,Zr)_3$

Table 2: Calculated and optimized formation enthalpies of the intermetallic phases of the Fe–Zr and Fe–Sn systems from the present work compared with the values available in the literature

		ΔH_f (kJ/mol-at)			
Composition		***C*15**	***C*36**	***C*16**	***E*1a**
Fe_2Zr	**This work - calc**	**-27.89**	**-26.01**	**-13.19**	**-11.43**
	This work - opt	**-28.83**	**-23.07**	**-14.25**	**-11.76**
	Ref. [56]	-30.15	—	-9.88	-9.61
	Ref. [13]	-28.10	—	-16.1	-14.34
	Ref. [9]	-27.10	—	-13.6	-11.75
	Ref. [54]	-24.40	—	—	—
		ΔH_f (kJ/mol-at)			
Composition		**Fe_5Sn_3**	**Fe_3Sn_2**	**FeSn**	**$FeSn_2$**
	This work - calc	**2.79**	**-6.26**	**-10.93**	**-10.36**
	This work - opt	**2.79**	**-6.26**	**-12.32**	**-12.24**
	Ref. [30]	—	—	-23	-29
	Ref. [29]	—	—	-28	-24

Table 3: Calculated mixing enthalpies of the binary solid solutions from the present work.

		ΔH_{mix} (kJ/mol-at)				
Composition (at. %Zr)		**0.06**	**0.25**	**0.50**	**0.75**	**0.94**
Fe-Zr	**This work - fcc**	**5.02**	**11.88**	**14.02**	**8.11**	**1.91**
	This work - bcc	**7.71**	**15.07**	**12.81**	**4.50**	**2.34**
	This work - hcp	**5.05**	**11.26**	**9.76**	**4.21**	**1.52**
Fe-Sn	**This work - fcc**	**2.51**	**5.06**	**7.75**	**5.94**	**3.08**
	This work - bcc	**2.60**	**5.12**	**9.47**	**8.19**	**1.81**

Table 4: Optimized thermodynamic parameters for the Fe–Sn system from the present work

Phase	**Parameters (J/mol)**
Liquide	${}^0L_{Fe,Sn}$ = 21340
	${}^1L_{Fe,Sn}$ = – 6345
	${}^2L_{Fe,Sn}$ = – 5518
fcc	${}^0L_{Fe,Sn}$ = 23510
bcc	${}^0L_{Fe,Sn}$ = 30011+5.31*T
	${}^1L_{Fe,Sn}$ = – 24443
Fe_5Sn_3	$G_{Fe:Sn}$ = – 65017+23.66*T+5*GHSERFE+3*GHSERSN
Fe_3Sn_2	$G_{Fe:Sn}$ = – 60284+32.45*T+3*GHSERFE+2*GHSERSN
FeSn	$G_{Fe:Sn}$ = – 34941+22.60*T+GHSERFE+GHSERSN
$FeSn_2$	$G_{Fe:Sn}$ = – 47510+33.63*T+GHSERFE+2*GHSERSN

Table 5: Optimized thermodynamic parameters for the Fe–Zr system from the present work

Phase	Parameters (J/mol)
Liquid	${}^0L_{Fe,Zr}$ = – 70236 ${}^1L_{Fe,Zr}$ = – 3000
fcc	${}^0L_{Fe,Zr}$ = 60000
bcc	${}^0L_{Fe,Zr}$ = 40000-14.02*T ${}^1L_{Fe,Zr}$ = 50000
hcp	${}^0L_{Fe,Zr}$ = 25045 ${}^2L_{Fe,Sn,Zr}$ = -700000
*C*15 $(Fe, Zr)_1 (Fe, Zr)_2$	$G_{Fe:Fe}$ = +35876 +3*GHSERFE $G_{Fe:Zr}$ = +227815+2*GHSERZR+GHSERFE $G_{Zr:Fe}$ = – 105104+12.44*T+GHSERZR+2*GHSERFE $G_{Zr:Zr}$ = +88549+3*GHSERZR ${}^0L_{Fe,Zr:Fe} = {}^0L_{Zr:Fe,Zr}$ = – 22000
*C*36 $(Fe, Zr)_4 (Fe, Zr)_4 (Fe, Zr)_{16}$	$G_{Fe:Fe:Fe}$ = 290739+24*GHSERFE $G_{Zr:Fe:Fe}$ = – 279300+20*GHSERFE+4*GHSERZR $G_{Fe:Zr:Fe}$ = – 253849+20*GHSERFE+4*GHSERZR $G_{Zr:Zr:Fe}$ = – 700972+107.2*T+16*GHSERFE+8*GHSERZR $G_{Fe:Fe:Zr}$ = 1791026+8*GHSERFE+16*GHSERZR $G_{Zr:Fe:Zr}$ = 1419297+4*GHSERFE+20*GHSERZR $G_{Fe:Zr:Zr}$ = 1375455+4*GHSERFE+20*GHSERZR $G_{Zr:Zr:Zr}$ = 618997+24*GHSERZR ${}^0L_{Zr:Fe,Zr:Fe}$ = – 350000
*C*16 $(Fe, Zr)_1 (Fe, Zr)_2$	$G_{Fe:Fe}$ = +106333+3*GHSERFE $G_{Zr:Fe}$ = +31049+GHSERZR+2*GHSERFE $G_{Fe:Zr}$ = – 52050+7.92*T+GHSERFE+2*GHSERZR $G_{Zr:Zr}$ = 94770+3*GHSERZR ${}^0L_{Fe:Fe,Zr}$ = – 218320 ${}^0L_{Fe,Zr:Zr}$ = – 99416
*E*1a $(Fe, Zr)_1 (Fe, Zr)_3$	$G_{Fe:Fe}$ = +160799+4*GHSERFE $G_{Zr:Fe}$ = 198436+GHSERZR+3*GHSERFE $G_{Fe:Zr}$ = – 56350+7.37*T+GHSERFE+3*GHSERZR $G_{Zr:Zr}$ = +60769+4*GHSERZR

Table 6: Composition and annealing treatments of the Fe–Sn–Zr samples prepared in this work

Nominal composition	Heat treatment	Structure (Space group)	Lattice parameters (Rietveld)	Composition (EPMA)
$Fe_{0.7}Sn_{2.3}Zr_5$	8h at 1350 °C	W_5Si_3 (*I*4/*mcm*)	*a*=11.170 Å; *c*=5.490 Å	$Zr_{60.7}Sn_{30.1}Fe_{9.2}$
$Fe_{0.7}Sn_{2.3}Zr_5$	7 days at 1000 °C	W_5Si_3 (*I*4/*mcm*) Mn_5Si_3 (*P*6$_3$/*mcm*) ?	*a*=11.166 Å; *c*=5.481 Å *a*=8.473 Å; *c*=5.780 Å ?	$Zr_{61.4}Sn_{29.3}Fe_{9.3}$ $Zr_{60.1}Sn_{38.7}Fe_{1.2}$ $Zr_{33.4}Sn_{0.2}Fe_{66.4}$
$Fe_{0.85}Sn_{2.15}Zr_5$	7 days at 1000 °C	W_5Si_3 (*I*4/*mcm*) Mn_5Si_3 (*P*6$_3$/*mcm*) ?	*a*=11.163 Å; *c*=5.480 Å *a*=8.473 Å; *c*=5.780 Å ?	$Zr_{62.4}Sn_{28.3}Fe_{9.3}$ $Zr_{61.9}Sn_{37.7}Fe_{0.4}$ $Zr_{33.8}Sn_{0.2}Fe_{66.0}$
$Fe_1Sn_2Zr_5$	7 days at 1000 °C	W_5Si_3 (*I*4/*mcm*) Mn_5Si_3 (*P*6$_3$/*mcm*) ?	*a*=11.168 Å; *c*=5.482 Å *a*=8.481 Å ; *c*=5.781 Å ?	$Zr_{60.6}Sn_{30.6}Fe_{8.8}$ $Zr_{60.3}Sn_{39.2}Fe_{0.5}$ $Zr_{32.9}Sn_{0.2}Fe_{66.9}$

Table 7: Calculated and optimized formation enthalpies of the Fe–Sn–Zr ternary phases

Phase	Space group	ΔH_f (kJ/mol) - calc	ΔH_f (kJ/mol) - opt
$Fe_{36.36}Sn_{36.36}Zr_{27.27}$ (*N*)	*Pnma*	-27.623	-28.970
$FeSn_2Zr_6$ (θ)	*P*-62*m*	-39.437	-40.881
Fe_6Sn_6Zr	*P*6/*mmm*	-8.789	-8.940
$Zr_5Sn_{2.3}Fe_{0.7}$	*I*4/*mcm*	-40.035	-41.657
$Fe_{17.39}Sn_{43.47}Zr_{39.13}$ (*X''*)	*Cmc*2_1	-39.860	-41.280
$Fe_{17.65}Sn_{39.22}Zr_{43.13}$ (*X'*)	Unknown	—	-47.605
$Fe_{56.24}Sn_{28.13}Zr_{15.63}$ (*Y*)	Unknown	—	-18.146

Table 8: Optimized thermodynamic parameters for the Fe–Sn–Zr system from the present work

Phase	Parameters (J/mol)
*C*14 $(Fe,Sn,Zr)_4$ $(Fe,Sn,Zr)_2(Fe,Sn,Zr)_6$	$G_{Fe:Sn:Zr}$ = 846468+4*GHSERFE+2*GHSERSN+6*GHSERZR $G_{Zr:Sn:Fe}$ = – 305871+6*GHSERFE+2*GHSERSN+4*GHSERZR $G_{Sn:Zr:Fe}$ = 156184+6*GHSERFE+4*GHSERSN+2*GHSERZR $G_{Sn:Fe:Zr}$ = – 44458+2*GHSERFE+4*GHSERSN+6*GHSERZR $G_{Zr:Fe:Sn}$ = – 120232+2*GHSERFE+6*GHSERSN+4*GHSERZR $G_{Fe:Zr:Sn}$ = 665830+4*GHSERFE+6*GHSERSN+2*GHSERZR
*C*15 $(Fe,Sn,Zr)_2(Fe,Sn,Zr)_1$	${}^0L_{Fe:Sn,Zr}$ = – 110000
*C*36 $(Fe,Sn,Zr)_4$ $(Fe,Sn,Zr)_4(Fe,Sn,Zr)_{16}$	$G_{Fe:Sn:Zr}$ = 975964+4*GHSERFE+2*GHSERSN+6*GHSERZR $G_{Zr:Sn:Fe}$ = – 410268 –109*T+6*GHSERFE+2*GHSERSN+4*GHSERZR $G_{Sn:Zr:Fe}$ = – 368546+6*GHSERFE+4*GHSERSN+2*GHSERZR $G_{Sn:Fe:Zr}$ = 1175979+2*GHSERFE+4*GHSERSN+6*GHSERZR $G_{Zr:Fe:Sn}$ = 1135254+2*GHSERFE+6*GHSERSN+4*GHSERZR $G_{Fe:Zr:Sn}$ = 1205127+4*GHSERFE+6*GHSERSN+2*GHSERZR ${}^0L_{Zr:Sn,Zr:Fe}$ = – 398285 + 75*T
$Fe_{36,36}Sn_{36,36}Zr_{27,27}$ (*N*) $(Fe)_{16}(Sn)_{16}(Zr)_{12}$	*G*= – 1420604 – 175*T+16*GHSERFE+16*GHSERSN+12*GHSERZR
$FeSn_2Zr_6$ (θ) $(Fe)_1(Sn)_2(Zr)_6$	*G*= – 368233 +1*GHSERFE+2*GHSERSN+6*GHSERZR
Fe_6Sn_6Zr $(Fe)_6(Sn)_6(Zr)_1$	*G*= – 170972 – 34*T+6*GHSERFE+6*GHSERSN+1*GHSERZR
$Zr_5Sn_{2,3}Fe_{0,7}$ $(Fe)_3(Sn)_9(Zr)_{20}$	*G*= – 1360910 – 148*T+3*GHSERFE+9*GHSERSN+20*GHSERZR
$Fe_{14.39}Sn_{43.47}Zr_{39.13}$ (*X''*) $(Fe)_8(Sn)_{20}(Zr)_{18}$	*G*= – 1971900 – 160*T+8*GHSERFE+20*GHSERSN+18*GHSERZR
$Fe_{17,65}Sn_{39,22}Zr_{43,13}$ (*X'*) $(Fe)_9(Sn)_{20}(Zr)_{22}$	*G*= – 2510000 +9*GHSERFE+20*GHSERSN+22*GHSERZR
$Fe_{36,36}Sn_{36,36}Zr_{27,2}$ (*Y*) $(Fe)_{18}(Sn)_9(Zr)_5$	*G*= – 745000 +18*GHSERFE+9*GHSERSN+5*GHSERZR